The Impact of Boundary Conditions on the Upstream Spreading of Bottom-Trapped Plumes

Ricardo P. Matano

College of Earth, Ocean, and Atmospheric Science, Oregon State University, Corvallis, Oregon

Elbio D. Palma

Departamento de Física, Universidad Nacional del Sur, and Instituto Argentino de Oceanografía, Bahia Blanca, Argentina

ABSTRACT

This study shows that simulations of bottom-trapped plumes in periodic or closed domains generate a spurious cyclonic current that arrests the natural tendency of the plume to move upstream. Furthermore, it also shows that attempts to obstruct the upstream spreading lead to a bias of the fundamental characteristics of the plume.

1. Introduction

Upstream spreading, which is spreading in the direction opposite to that of propagation of the coastal-trapped waves, has been a common trait of numerical simulations of bottom-trapped plumes (BTP) (e.g., Garvine 1999; Chapman and Lentz 1994; Kourafalou et al. 1996). In fact, upstream spreading, which had been deemed a spurious artifact of numerical simulations, had been so "pervasive" that a wide variety of techniques have been used to suppress it (Garvine 2001; Yankovsky 2000). Recently, we argued that the upstream spreading of BTPs is a consequence of the geostrophic adjustment of a buoyant discharge and not a model artifact (Matano and Palma 2010a,b; hereafter MP10a and MP10b). Furthermore, we also argued that upstream spreading should always be observed and can only be prevented by external factors such as a downstream mean flow, tides, or wind stress forcing. These arguments notwithstanding, Pimenta et al. (2011; hereafter P11) recently presented numerical simulations of BTP showing no upstream spreading. They argued that a "realistic" model setup including a long estuary, a canyon at the mouth of the estuary, and the use of
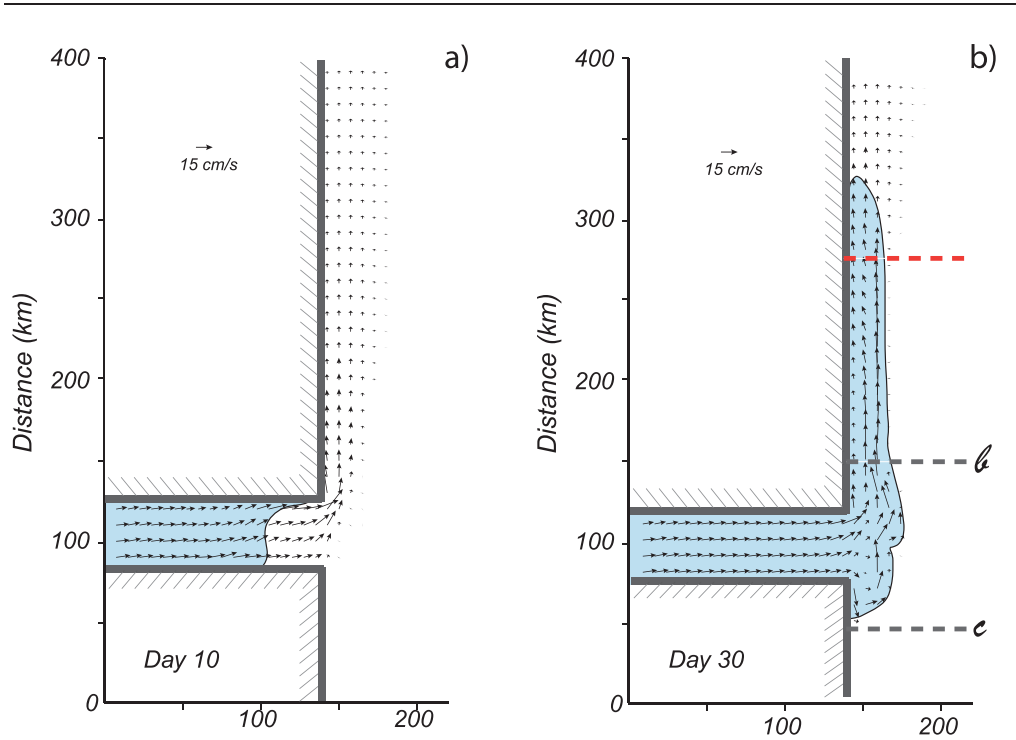
periodic (cyclic) boundary conditions prevents this phenomenon. In this article, we show that the lack of upstream spreading in the P11 simulations is an artifact created by the model's boundary conditions—specifically, that simulations in periodic or closed domains develop a spurious cyclonic current that arrests the natural tendency of the BTP to move upstream. This conclusion is also applicable to rotating tank experiments using periodic conditions (e.g., Avicola and Huq 2002) or conducted in semienclosed domains (e.g., Lentz and Helfrich 2002). We also show that the inhibition of upstream spreading has an adverse effect on estimates of the plume's characteristics, for example, width, alongshelf extent, buoyancy transport, etc. Our discussion is based on the results of a suite of process-oriented numerical simulations. In the following sections we describe the model setup, discuss the numerical experiments, and present our final conclusions.

2. Model setup

The numerical model used in this study is the Princeton Ocean Model (Blumberg and Mellor 1987). The model domain is set in the Southern Hemisphere and consists of a rectangular basin 400 km long (y direction) and 80 km wide (x direction). The grid resolution is 2.5 km in the y direction, 1.25 km in the x direction, and 25 sigma levels in the vertical. The bottom topography consists of a shelf with a constant slope and no meridional

Corresponding author address: Dr. Ricardo Matano, College of Earth, Ocean, and Atmospheric Science, Oregon State University, Ocean Admn. Bldg. 104, Corvallis, OR 97331-5503.
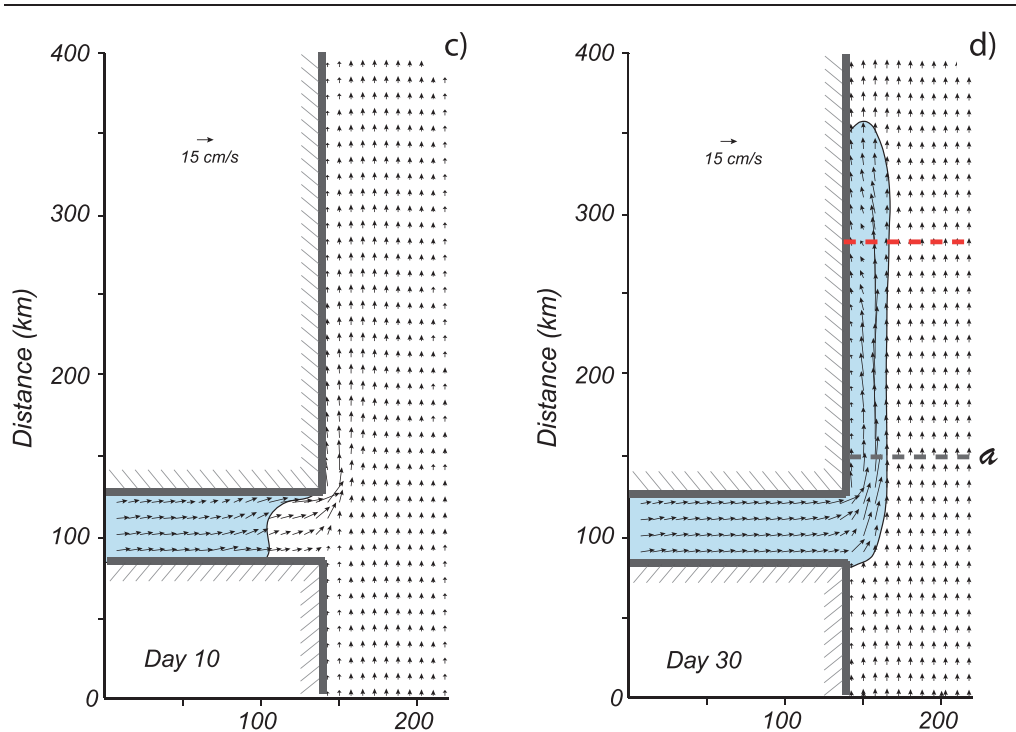E-mail: rmatano@coas.oregonstate.edu

FIG. 1. Snapshots of the surface density anomalies (color) and the surface velocity vectors for (top) EXP1 (open boundaries) and (bottom) EXP2 (cyclic boundary conditions) and for day (left) 10 and (right) 30. Surface density anomalies vary between -1 and 0 kg m^{-3} with the outer boundary indicating the 0.0 kg m^{-3} contour. The red dashed line in (b),(d) marks the location of the snapshots shown in Fig. 4.
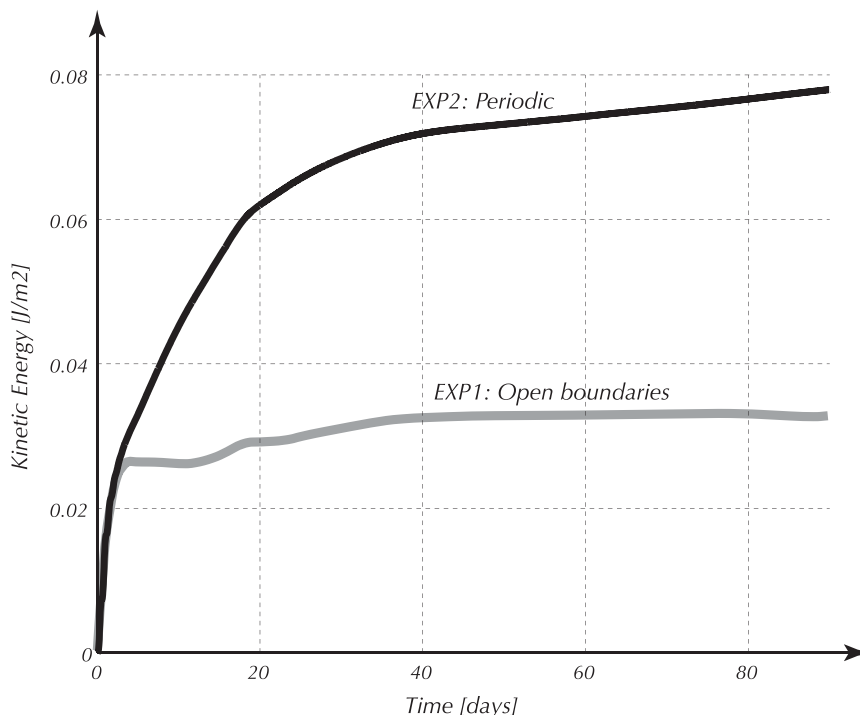
FIG. 2. Time evolution of the basin-averaged kinetic energy $(J\,m^{-2})$ for EXP1 (open boundaries, gray line) and EXP2 (periodic boundaries, black line).

variations. Bottom friction is parameterized with a quadratic friction law with a variable drag coefficient. A recursive scheme is used for the advection terms (Smolarkiewicz and Grabowski 1990). We present experiments in periodic, open, and closed domains. At the open boundaries we use the same conditions as MP10a, which follow the recommendations of Palma and Matano (1998, 2000). We use the Flather (1974) radiation scheme for the barotropic variables (depth-averaged velocities and sea surface elevation), the Orlanski (1976) radiation condition for the baroclinic velocities, and an advection scheme for the density. All experiments include a solid western boundary. The inlet in all experiments, except EXP5, is centered at $y = 100$ km, with a width of 34 km and a depth of 15 m. The depth of the basin is 15 m at the coast and increases linearly across shore with a bottom slope of 2×10^{-3}. The Rossby number of the discharge is ~ 0.013, a value similar to that used by P11. The buoyancy source is imposed in the continuity equation following the scheme of Kourafalou et al. (1996). Water of a prescribed density is introduced uniformly throughout the top half of the water column in the grid cells representing the river mouth. The discharge has a density anomaly of -1.0 kg m^{-3} and a volume flux of 24 000 m^3 s^{-1}. The ocean is initially quiescent and of constant reference density ρ_o; the Coriolis parameter is set at $f = -10^{-4}$ s^{-1}; the coefficients of vertical eddy

viscosity K_M and diffusivity K_H are computed using the Mellor–Yamada 2.5 closure scheme. A more detailed description of the results of EXP1, which is our benchmark case, and its sensitivity to model configuration (bottom slope, mixing scheme, magnitude of the discharge, etc.) can be found in MP10a.

3. Results

To demonstrate the influence of periodic domains on the upstream spreading of BTP, we ran two experiments differing only in the boundary conditions imposed at the cross-shelf boundaries; EXP1 uses the open boundary conditions described in MP10a while EXP2 uses periodic conditions. To facilitate the comparison with the results of P11 we set the horizontal diffusion of both experiments to zero. The experiments are started at rest and are integrated for 30 days.

The results of EXP1 are illustrated with two snapshots taken at day 10 and day 30 (Figs. 1a,b). Immediately after the release of the discharge, barotropic coastal-trapped waves propagate the volume anomaly into the downstream region establishing a cross-shelf barotropic pressure gradient and a geostrophically balanced current. At day 10, the discharge had generated an alongshelf barotropic current that widens in the downstream direction because of the effects of bottom friction
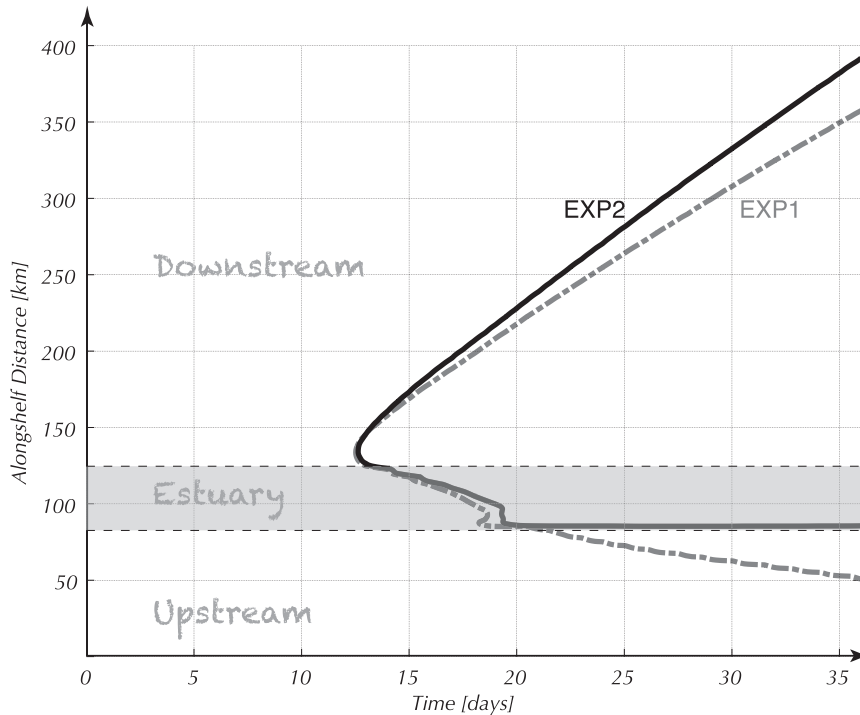
FIG. 3. Time evolution of the position of the nose of the plumes of EXP1 (gray dotted line) and EXP2 (black solid line) in the alongshelf direction. The gray-shaded area marks the location of the estuary. The nose of the plume corresponds to the 0.0 density anomaly contour 15 km from the coast.

(Fig. 1a). Using the arrested topographic wave theory (Csanady 1978) we can estimate the width W of the jet at the downstream boundary as

$$W \sim \sqrt{L_y r / f \alpha},$$

where W is the cross-shelf width of the jet at a distance L_y from the mouth of the estuary (~ 300 km), r is the coefficient of bottom friction ($\sim 10^{-3}$), f is 10^{-4}, and α is the bottom slope (2×10^{-3}). The estimated value of W is 38 km, which is close to the observed value of ~ 30 km (Fig. 1a). At day 10 the density anomaly has not yet left the estuary, therefore the upstream region remains undisturbed (Fig. 1a). During the course of the following days the barotropic current advects the density anomaly out of the estuary and toward the downstream region (Fig. 1b). Thus, an observer of the spinup process located at a downstream point will notice that the change of the velocity field precedes the change of the density field, which is akin to a spin up of deep circulation by deep water formation (e.g., Kawase 1987). The arrival of the density anomaly to a particular location modifies the vertical and horizontal structure of the barotropic mean flow, leading to a narrower and surface-intensified coastal jet. The surface velocities within the plume are

~ 0.25 m s^{-1} and outside of the plume they decrease to 0.05 m s^{-1}. Downstream of the plume's nose the flow remains wider and less intense (Fig. 1b). The spinup in the upstream region is quite different because the progression of the density anomaly is not preceded by a barotropic signal (MP10a). The intrusion of the density anomaly generates an unbalanced cross-shelf baroclinic pressure gradient that leads to a self-sustaining upstream flow (MP10a). The upstream spreading is slower than the downstream spreading but it is a robust phenomenon that, for this particular model configuration, diverts approximately half of the buoyancy into the upstream direction (MP10a).

The spinup of EXP2 is substantially different from the spinup of EXP1 (Fig. 1c and Fig. 1d). The coastal-trapped waves do not radiate to infinity but reenter the domain through the upstream boundary, thus setting up a barotropic pressure gradient that leads to the development of a spurious downstream current (Fig. 1c). Since the energy of the discharge cannot escape the domain, the speed of the spurious downstream current increases steadily with time. Thus, while the average kinetic energy of EXP1 reaches a steady state in a few days, the kinetic energy of EXP2 has a fast adjustment that lasts approximately three weeks, after which it keeps growing at
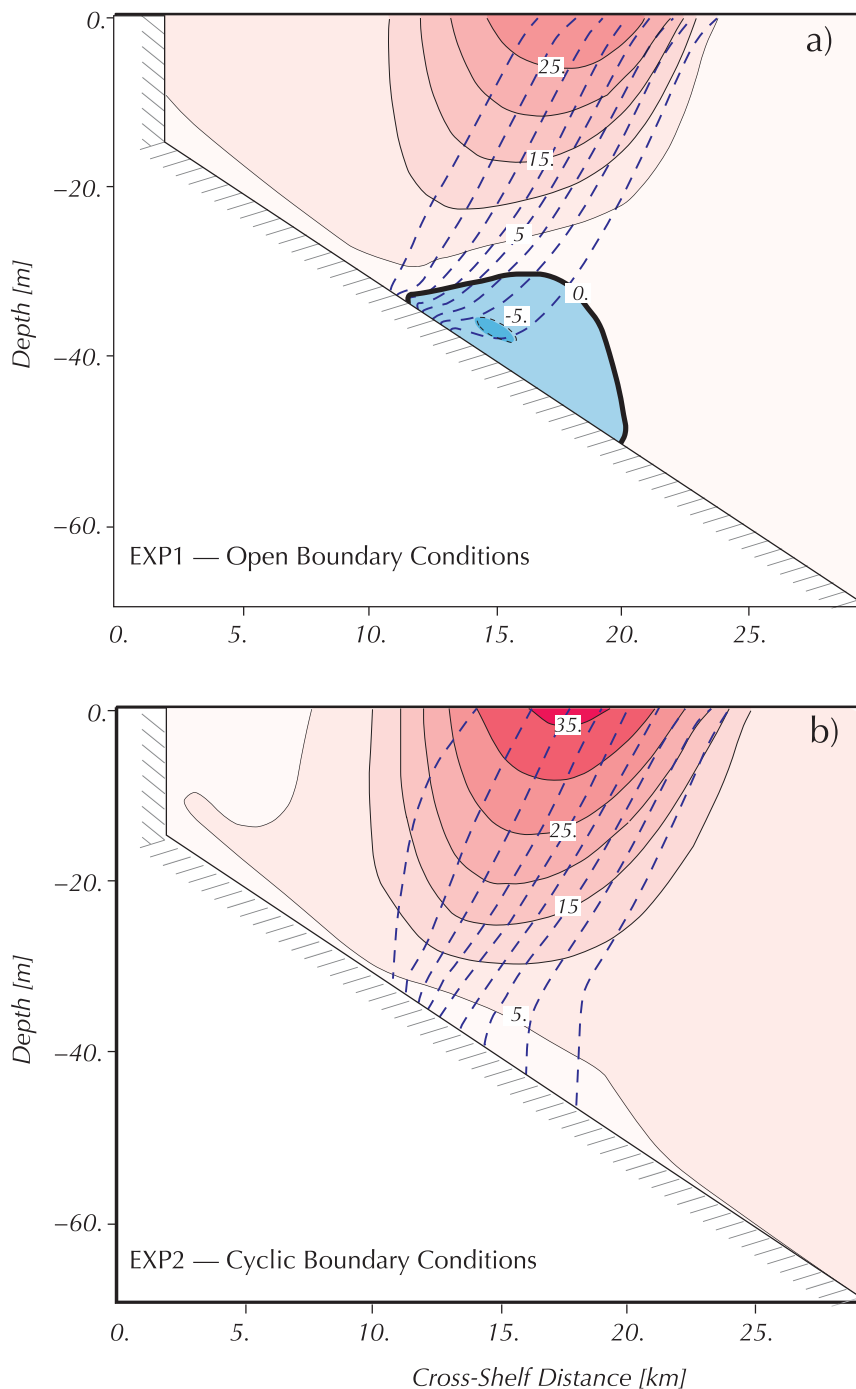
FIG. 4. Snapshots of the alongshelf velocities (color) and density anomalies (blue dashed lines) at day 30 in (a) EXP1 (open boundaries) and (b) EXP2 (cyclic boundaries). The location of the cross-shelf sections is shown in Fig. 1 (red dashed lines).

a slower rate (Fig. 2). After 90 days of numerical integration the kinetic energy of EXP2 is approximately three times larger than that of EXP1, and the difference keeps growing. Thus, the use of cyclic boundary

conditions not only generates a spurious mean flow but also a mean flow that is constantly growing in time. At day 10 the plume has not yet left the estuary, therefore, although the velocity field of EXP2 is markedly different
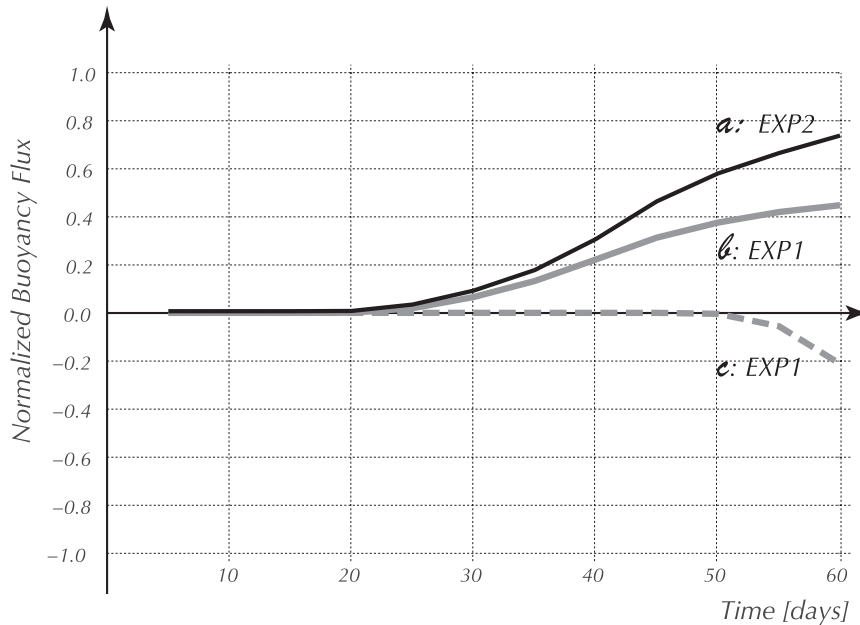
FIG. 5. Normalized buoyancy fluxes of EXP1 (gray solid and dashed lines) and EXP2 (black solid line). The buoyancy fluxes were calculated at the cross sections labeled a, b, and c in Fig. 1.

from that in EXP1, the density signature of both plumes are almost identical. The density differences between the two experiments start to show after the plume leaves the estuary. The spurious downstream current arrests the upstream development of the discharge and advects the entire density anomaly in the downstream direction (Fig. 1d). The plume of EXP2 extends farther downstream than that of EXP1. At day 35, for example, the noses of the two plumes are more than 30 km apart and the distance between them keeps growing (Fig. 3).

The differences between the two experiments are further illustrated in Fig. 4, which shows the vertical structure of the velocity fields in a downstream cross-shelf section. A strong baroclinic structure with a surface downstream flow overlying a deep countercurrent characterizes EXP1 (Fig. 4a). This countercurrent produces an upslope flow in the bottom boundary layer that advects denser waters toward the coast producing the observed bending of the isopycnals (Fig. 4a). This velocity/density structure is characteristic of bottom-trapped plumes and the dynamical mechanisms that generate it have been described in detail in previous studies (e.g., Chapman and Lentz 1994). In contrast, EXP2 shows a more homogenous vertical velocity profile that extends from the surface to the bottom (Fig. 4b), and that is similar to that shown by P11 (their Fig. 3c). As noted above, the velocities of EXP2 are higher than those of EXP1—surface velocities in EXP2 have a peak of 0.35 m s^{-1} while those in EXP1 have a peak of 0.27 m s^{-1}. The

difference between experiments is almost three times larger for the vertically averaged velocities on account of the different vertical structures of the jets. The spurious flow generated during the spinup of EXP2 arrests the development of the deep countercurrent and widens the density front. The different density/velocity structures of EXP1 and EXP2 lead to larger downstream buoyancy flux in EXP2, which is more than 50% larger than that of EXP1 (Fig. 5). This difference is partly attributed to differences in the velocity fields and partly to the fact that in EXP1 a significant portion of the buoyancy flux is diverted toward the upstream region. In EXP1 the upstream portion of the plume reaches the upstream cross-shelf section at day 50, whence the buoyancy flux starts to grow linearly in time (Fig. 5).

We also investigated the impact of closed or semi-enclosed basins on the characteristics of BTPs. These types of domains are commonly used in laboratory simulations of gravity currents (e.g., Whitehead and Chapman 1986; Lentz and Helfrich 2002) and have been used in numerical simulations (e.g., Chao and Boicourt 1986). Our first set of simulations, which focuses on flat-bottomed basins, consists of two experiments that differ only on the boundary conditions. The EXP3 imposes solid walls and EXP4 uses open boundary conditions at the cross-shelf and offshore boundaries. There are substantial differences between the results of the two experiments (Fig. 6). The plume of EXP3 shows no upstream spreading, is narrower, and extends farther

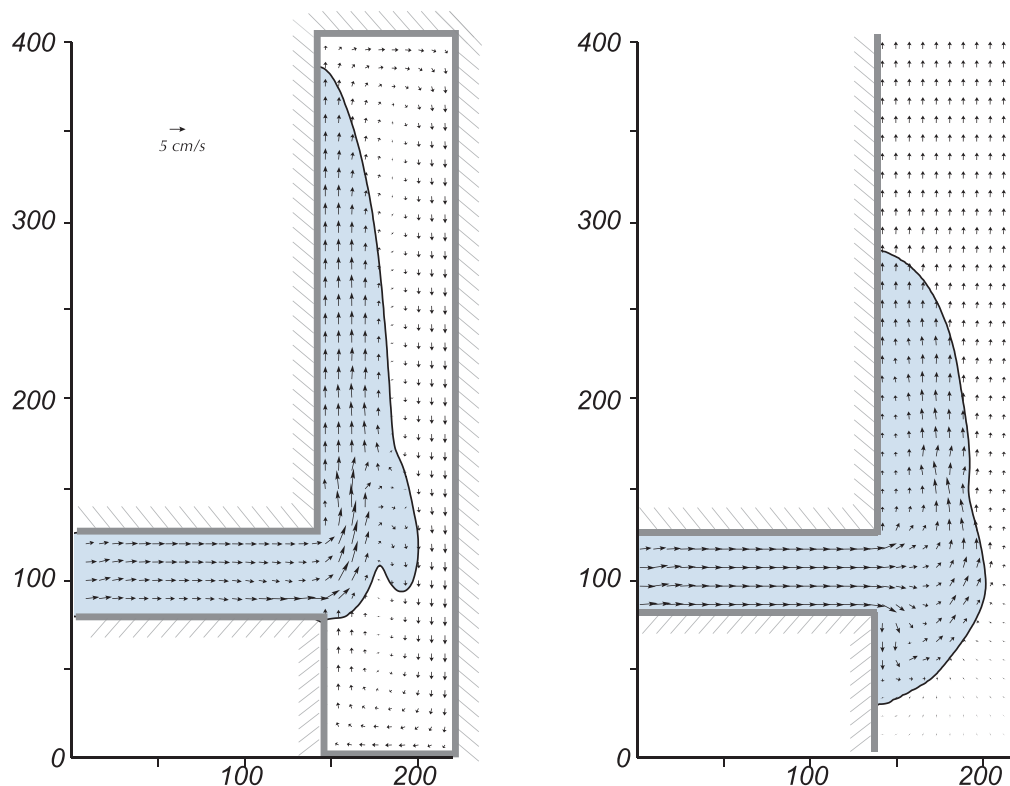## a) EXP3 — Closed boundaries

b) EXP4 — Open boundaries

FIG. 6. Snapshots of the surface density anomalies (color) and the depth-averaged velocities at day 90 in (a) EXP3 (closed boundaries) and (b) EXP4 (open boundaries). Surface density anomalies vary between -1 and $0 \, \mathrm{kg \, m^{-3}}$ with the outer boundary indicating the $0.0 \, \mathrm{kg \, m^{-3}}$ contour. Both experiments were conducted in a flat-bottomed basin.

downstream than that of EXP4. In EXP3 the barotropic waves triggered by the discharge do not reenter through the upstream boundary, as in the periodic case, but are instead recirculated around the solid walls. The end effect, however, is similar: the barotropic waves set up a spurious cross-shelf pressure gradient and a cyclonic recirculation cell that arrests the upstream spreading and advects the plume farther downstream of where it should be. We also did experiments using a sloping bottom (not shown). In those experiments the bottom topography hinders the recirculation of the coastal-trapped waves thus allowing the upstream propagation of the plume.

Lentz and Helfrich (2002) presented a series of tank experiments in which the discharge flows from an inlet in a wall located at the upstream end of the domain, thus explicitly inhibiting upstream spreading. To assess how this set up impacts the plume's characteristics we conducted two experiments: EXP5, which emulates

the discharge conditions of Lentz and Helfrich in an otherwise open basin, and EXP6, which has discharge flowing perpendicular to the shelf, thus allowing upstream spreading. Following MP10a these experiments include a sloping bottom, a narrower inlet, and a horizontal diffusion of density of $20 \, \mathrm{m^2 \, s^{-1}}$. The new experiments were started at rest and integrated for 90 days. The plume of EXP5 spreads downstream and laterally (Fig. 7a). Lateral spreading, which is generated by the same mechanism mediating upstream spreading, is also apparent in the experiments of Lentz and Helfrich (2002) (e.g., see their Fig. 5). The EXP6 demonstrates the impact of upstream spreading on the downstream region (Fig. 7b). In the downstream region the plume of EXP6 is narrower than that of EXP5 and moves at a slower rate. These differences are related to the lack of upstream spreading in EXP5 and are quantified by the buoyancy balances, which indicate in EXP5 that approximately 70% of the buoyancy inflow is funneled

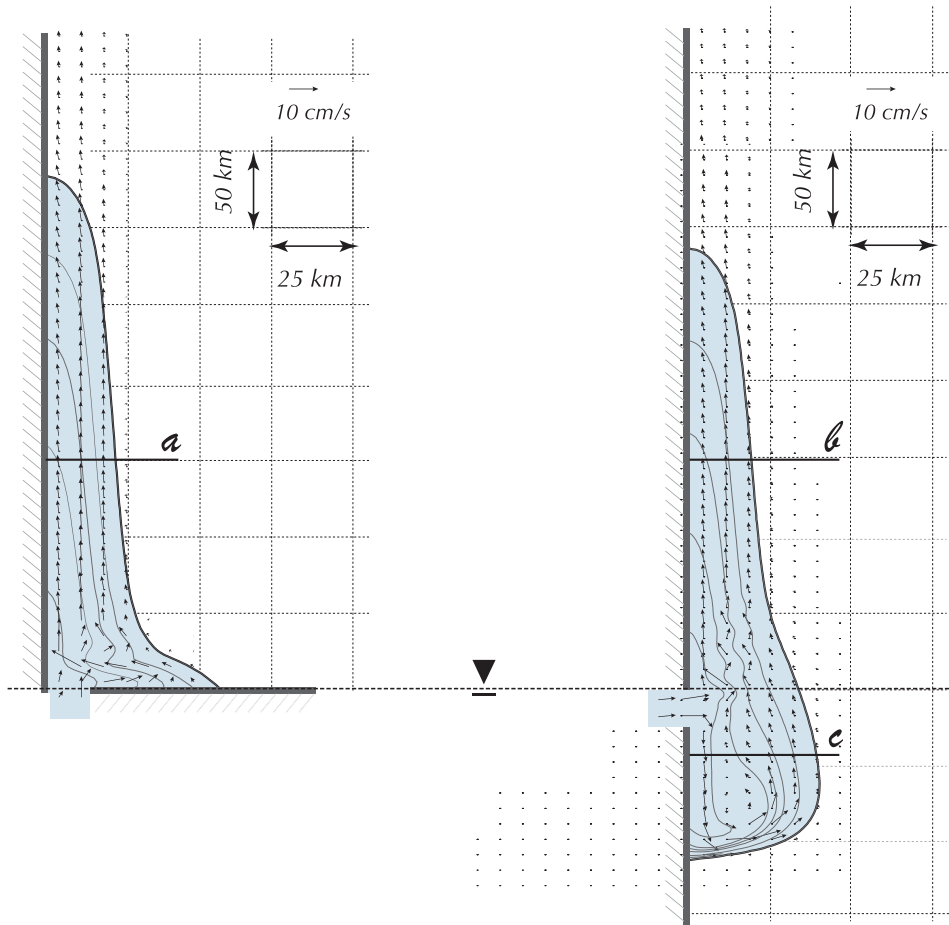a) EXP5 — Semi-Closed boundaries   b) EXP6 — Open boundaries

FIG. 7. Snapshots of the surface density anomaly (color) and surface velocities at day 60 in (a) EXP5 (semienclosed boundaries), and (b) EXP6 (open boundaries). Surface density anomalies vary between 0 and −1 kg m^{-3}, and are contoured at −0.2 kg m^{-3} intervals.

downstream while in EXP6 less than 40% of that inflow is diverted downstream (Fig. 8). That is, for this particular model configuration, the downstream buoyant discharge is reduced approximately 50% when upstream spreading is allowed. We also did variations of EXP5 in a closed domain and different bottom slopes. In a flat-bottomed basin the plume is distorted by a cyclonic recirculation cell similar to that depicted in Fig. 6a. However, the inclusion of a sloping bottom prevents the coastal-trapped waves from reaching the nearshore region, therefore ameliorating their impact on the plume characteristics. Thus, we surmise that the lateral walls of the container did not significantly affect the experiments of Lentz and Helfrich (2002). However, the inclusion of a zonal wall close to the inlet has a strong influence on the downstream characteristics of the plume.

4. Conclusions

Periodic domains, which have been used in numerical studies and are frequently employed in laboratory simulations, are unsuitable for the study of BTP because they allow the development of a spurious current that changes the natural characteristics of the flow. Closed domains can potentially be affected by the same problem, although our simulations suggest that the inclusion of a slopping bottom ameliorates the impact of spurious motions over the nearshore region. The particular laboratory setup used by Lentz and Helfrich (2002) avoids some of the pitfalls of periodic and closed domains but the inhibition of upstream spreading distorts the plume characteristics. Thus, the scale analysis presented by Lentz and Helfrich (2002) should be modified to take
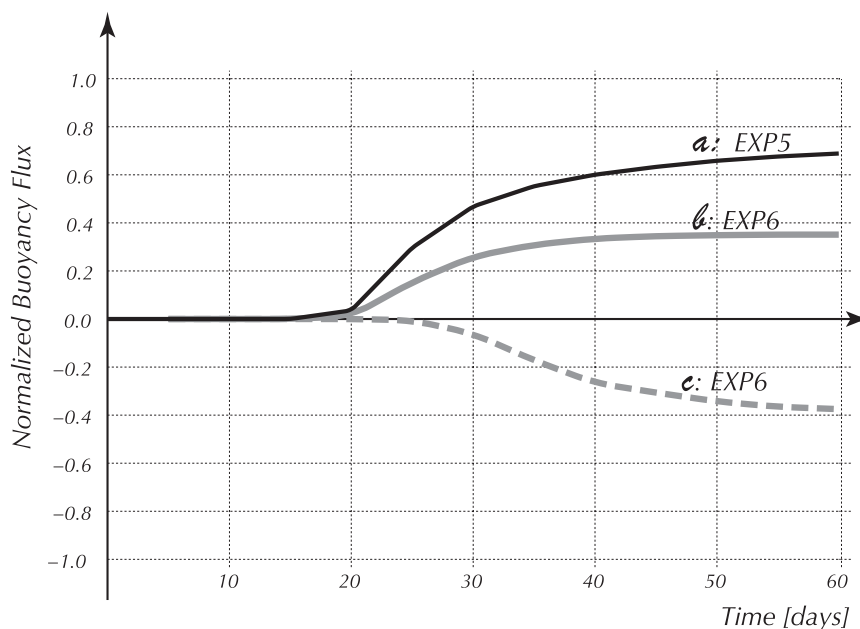
FIG. 8. Normalized buoyancy balances of EXP5 (black solid line) and EXP6 (gray solid and dotted lines). The location of cross sections a, b, and c are marked in Fig. 7.

into account that their estimates depend on the portion of the flow that is diverted downstream, and not on the total discharge through the inlet. This is not a minor point since the dependence of the downstream flow on the general characteristics of the discharge and the geometry of the basin has not yet been established.

In summary, we have shown that boundary conditions that artificially prevent the upstream spreading of bottom-trapped plumes have a deleterious effect on the plume characteristics and dynamics: upstream spreading subtracts a substantial portion of the buoyancy input from the downstream region, thus shaping the fundamental characteristics of the free flow.

REFERENCES

Avicola, G., and P. Huq, 2002: Scaling analysis for the interaction between a buoyant coastal current and the continental shelf: Experiments and observations. *J. Phys. Oceanogr., 32,* 3233–3248.

Blumberg, A. F., and G. L. Mellor, 1987: A description of a three-dimensional coastal ocean circulation model. *Three-Dimensional Coastal Ocean Models,* N. Heaps, Ed., Coastal Estuarine Science, Vol. 4, Amer. Geophys. Union, 1–16.

Chao, S.-Y., and W. C. Boicourt, 1986: Onset of estuarine plumes. *J. Phys. Oceanogr., 16,* 2137–2149.

Chapman, D. C., and S. J. Lentz, 1994: Trapping of a coastal density front by the bottom boundary layer. *J. Phys. Oceanogr., 24,* 1464–1479.

Csanady, G. T., 1978: The arrested topographic wave. *J. Phys. Oceanogr., 8,* 47–62.

Flather, R. A., 1974: A tidal model of the northwest European continental shelf. *Mem. Soc. Roy. Sci. Liege, Ser., 6,* 141–164.

Garvine, R. W., 1999: Penetration of buoyant coastal discharge onto the continental shelf: A numerical model experiment. *J. Phys. Oceanogr., 29,* 1892–1909.

——, 2001: The impact of model configuration in studies of buoyant coastal discharge. *J. Mar. Res., 59,* 193–225.

Kawase, M., 1987: Establishment of deep ocean circulation driven by deep-water production. *J. Phys. Oceanogr., 17,* 2294–2317.

Kourafalou, V. H., L.-Y. Oey, J. D. Wang, and T. N. Lee, 1996: The fate of river discharge on the continental shelf 1. Modeling the river plume and inner shelf coastal current. *J. Geophys. Res., 101* (C2), 3415–3434.

Lentz, S. J., and K. R. Helfrich, 2002: Buoyant gravity currents along a sloping bottom in a rotating fluid. *J. Fluid Mech., 464,* 251–278.

Matano, R. P., and E. D. Palma, 2010a: The upstream spreading of bottom-trapped plumes. *J. Phys. Oceanogr., 40,* 1631–1650.

——, and ——, 2010b: The spin-down of bottom-trapped plumes. *J. Phys. Oceanogr., 40,* 1651–1658.

Orlanski, I., 1976: A simple boundary condition for unbounded hyperbolic flows. *J. Comput. Phys., 21,* 251–269.

Palma, E. D., and R. P. Matano, 1998: On the implementation of open boundary conditions to a general circulation model: The barotropic mode. *J. Geophys. Res.,* **103** (C1), 1319–1341.

——, and ——, 2000: On the implementation of open boundary conditions for a general circulation model: The three-dimensional case. *J. Geophys. Res.,* **105** (C4), 8605–8627.

Pimenta, F. M., A. D. Kirwan Jr., and P. Huq, 2011: On the transport of buoyant coastal plumes. *J. Phys. Oceanogr.,* **41,** 620–640.

Smolarkiewicz, P. K., and W. W. Grabowski, 1990: The multidimensional positive definite advection transport algorithm: Nonoscillatory option. *J. Comput. Phys.,* **86,** 355–375.

Whitehead, J. A., and D. C. Chapman, 1986: Laboratory observations of a gravity current on a sloping bottom: The generation of shelf waves. *J. Fluid Mech.,* **172,** 373–399.

Yankovsky, A. E., 2000: The cyclonic turning and propagation of buoyant coastal discharge along the shelf. *J. Mar. Res.,* **58,** 585–607.